Linking Electrophysiological Metrics to Oxidative Metabolism: Implications for EEG–fMRI Association

Xiaole Z. Zhong[1,2], Hannah Van Lankveld[1,3], Alicia Mathew[1], and J. Jean Chen[1,2,3]

1- Rotman Research Institute at Baycrest, Toronto, ON, Canada;
2- Department of Medical Biophysics, University of Toronto, Toronto, ON, Canada;
3 - Department of Biomedical Engineering, University of Toronto, Toronto, ON, Canada.

Abstract

Resting-state functional magnetic resonance imaging (rs-fMRI) is widely used to study brain function, yet its biophysiological basis remains incompletely understood. Building on our recent work, we investigated how EEG activity and cerebral metabolic rate of oxygen ($CMRO_2$) are related to one another, and how they jointly underpin rs-fMRI metrics. Using a multimodal dataset with macrovascular correction applied to all rs-fMRI metrics, we first examined associations between EEG metrics and $CMRO_2$, then applied mediation analysis to evaluate how $CMRO_2$ mediates EEG–fMRI associations. We found that bandlimited EEG theta and alphafractional power was significantly associated with $CMRO_2$. Bandlimited EEG coherence was also associated with $CMRO_2$ across all the bands. Bandlimited EEG fractional power and coherence were also significantly associated with cerebral blood flow (CBF) and oxygen extraction fraction (OEF) in a manner that varied by frequency. EEG broadband temporal complexity was positively associated with $CMRO_2$ and EEG coherence was negatively associated with OEF. Notably, there are pronounced sex differences in these relationships, which suggests that the biophysical underpinnings of rs-fMRI are sex dependent. Moreover, the baseline metabolic and hemodynamic variables did partially mediate EEG–fMRI associations, with $CMRO_2$ serving as the primary mediator. However, most of the mediations are partial, highlighting the complex interplay among electrophysiological activity, oxidative metabolism, and hemodynamics. This study advances our understanding of the biophysical basis of rs-fMRI and provides a foundation for developing sex-specific diagnostic and therapeutic strategies for neurological disorders.

1 Introduction

Resting-state functional magnetic resonance imaging (rs-fMRI), most commonly based on the blood-oxygenation level-dependent (BOLD) contrast, leverages spontaneous brain activity (Biswal et al., 1995) to investigate brain function in health and disease. Most rs-fMRI studies focus on connectivity analysis, with BOLD signal power used to characterize the temporal variability of brain signals underlying connectivity measures ((Kannurpatti et al., 2011). More recently, non-linear metrics, particularly entropy, have provided novel insights into the relationship between rs-fMRI signal complexity and cognitive performance (Z. Wang, 2021). Despite the growing number of metrics proposed as markers of neuronal function, their clinical application remains limited, partly due to an incomplete understanding of the neuronal and metabolic mechanisms that underlie the rs-fMRI signal (Lee et al., 2013; Tsvetanov et al., 2021).

Since the early development of rs-fMRI, the preferred approach to clarify the interpretability of FC has been linking it to neuronal activity. Electrophysiological methods such as EEG and MEG are considered gold standards for measuring neuronal contributions. While some human studies have found correlations between EEG and fMRI FC, results have been inconsistent (Nentwich et al., 2020; Z. Wang, 2021; Wirsich et al., 2020, 2021). EEG power fluctuations may also contribute to FC measures, with associations reported across multiple frequency bands and networks (Liu et al., 2014; Neuner et al., 2014; Phadikar et al., 2025; Scheeringa et al., 2012). Oxidative metabolism ($CMRO_2$) and glucose metabolism (CMR_{glu}) are another key marker of neuronal activity due to the energy demands of neural processes. In particular, $CMRO_2$ is intricately linked to fMRI contrast, and rs-fMRI measurements has been linked to $CMRO_2$ both quantitatively qualitatively (Raichle et al., 2001) and quantitatively (Zhong, Van Lankveld, & Chen, 2025). However, it is unclear what the link between EEG and $CMRO_2$ is in the context of both contributing to fMRI. EEG signals arise from synchronized postsynaptic potentials directed toward scalp electrodes (Malmivuo et al., 1997; Sotero & Trujillo-Barreto, 2008; St. Louis et al., 2016), meaning any neuronal activity not producing synchronized postsynaptic currents is undetectable. Indeed, postsynaptic activity accounts for only ~74% of total ATP expenditure in humans (Attwell & Laughlin, 2001). Conversely, neuronal activity that does not elicit hemodynamic responses or changes in oxidative metabolism may be invisible to BOLD fMRI, as ATP can be produced via glucose metabolism alone with minimal hemodynamic involvement (Cholet et al., 1997; Vaishnavi et al., 2010). Although these studies have advanced our understanding of the neural underpinnings of FC, their interpretability remains limited, as suggested by our recent series of studies (Shokri-Kojori et al., 2019; Tomasi et al., 2013).

In our recent studies, we linked FC to both EEG FC (Zhong, Van Lankveld, Mathew, et al., 2025) and $CMRO_2$ measurements (Zhong, Van Lankveld, & Chen, 2025) individually. While we observed some similar association patterns as reported in previous studies, we also noted some substantial mismatches in both EEG–fMRI and $CMRO_2$–fMRI association. EEG and $CMRO_2$ both measure aspects of neuronal activity, but their biophysical underpinnings differ substantially. As we discussed previously, rs-fMRI reflects oxidative metabolism rather than total metabolism, and accordingly, resting-state $CMRO_2$ and CMRglu maps are distinct (Markello et al., 2022). One potential source of this discrepancy relates to aerobic and anaerobic glycolysis, which refers to glucose utilization exceeding that required for oxidative phosphorylation despite the presence of sufficient oxygen (Vaishnavi et al., 2010). This may explain why rs-fMRI measurements can diverge from $CMRO_2$ measurements. Furthermore, although the association between EEG and $CMRO_2$ is often assumed, it has not been systematically tested.

These considerations indicate that neither EEG–fMRI nor $CMRO_2$–fMRI association fully explain the rs-fMRI measurements. Post-synaptic activity, as measured by the EEG, is largely fueled by oxidative

metabolism (Attwell & Laughlin, 2001). The EEG–fMRI association is mediated by $CMRO_2$ as suggested by previous studies (Attwell & Laughlin, 2001). Conversely, more recent studies suggest discrepancies between EEG and rs-fMRI do not only imply non-neuronal contributions, but may also reflect EEG-invisible neuronal activity that nonetheless consumes oxygen (Tu et al., 2024), highlighting the need to test a $CMRO_2$ mediation framework to interpret the underpinnings of rs-fMRI. Furthermore, both $CMRO_2$-fMRI and EEG-fMRI associations are strongly influenced by sex as a fundamental phenotype (Zhong, Van Lankveld, & Chen, 2025; Zhong, Van Lankveld, Mathew, et al., 2025). Understanding sex effects is therefore critical for interpreting the role of $CMRO_2$ in rs-fMRI findings.

Sex differences in electrophysiological activity have been widely studied, both in terms of power (Corsi-Cabrera et al., 1993; Jausovec & Jausovec, 2010) and coherence (Duffy et al., 1996; Jausovec & Jausovec, 2010). Sex effects are also evident in cerebral metabolism and hemodynamics. Estrogen, the primary female sex hormone, significantly modulates multiple aspects of brain metabolism: it enhances glucose uptake by upregulating glucose transporter expression (Rettberg et al., 2014), increases the total cerebral metabolic rate of glucose (CMR_{glu}) by regulating glucose channel activity (Andreason et al., 1994; Rettberg et al., 2014), and promotes aerobic glycolysis by upregulating key glycolytic enzymes (Kostanyan & Nazaryan, 1992; Mannella & Brinton, 2006; Zhu et al., 2023; Znamensky et al., 2003). Consequently, females tend to exhibit higher glycolytic activity and potentially a greater reliance on aerobic glycolysis at rest (Goyal et al., 2019; Rettberg et al., 2014). In addition to metabolic effects, estrogen influences cerebral hemodynamics by modulating vascular tone and perfusion (White, 2002). This aligns with consistent reports that females show higher cerebral blood flow (CBF) but lower oxygen extraction fraction (OEF) compared to males (Aanerud et al., 2017; Gur & Gur, 1990). While findings on $CMRO_2$ differences are mixed, several studies have reported higher $CMRO_2$ values in females (Aanerud et al., 2017; Lu et al., 2011). Thus, neither the EEG-fMRI nor the $CMRO_2$-fMRI links are generalizable across sexes.

In this study, we acquired a multimodal dataset to investigate associations between EEG, $CMRO_2$. We also investigate the implications of this relationship for understanding fMRI metrics (**Fig. 1**), which were calculated incorporating our macrovascular correction pipeline to enhance the neuronal specificity. We examine how these relationships differ between sexes. By characterizing these interdependencies, this study aims to elucidate the electrophysiological and metabolic mechanisms underlying rs-fMRI, thereby advancing our understanding of brain function and informing the development of sex-specific diagnostic and therapeutic strategies for neurological disorders.

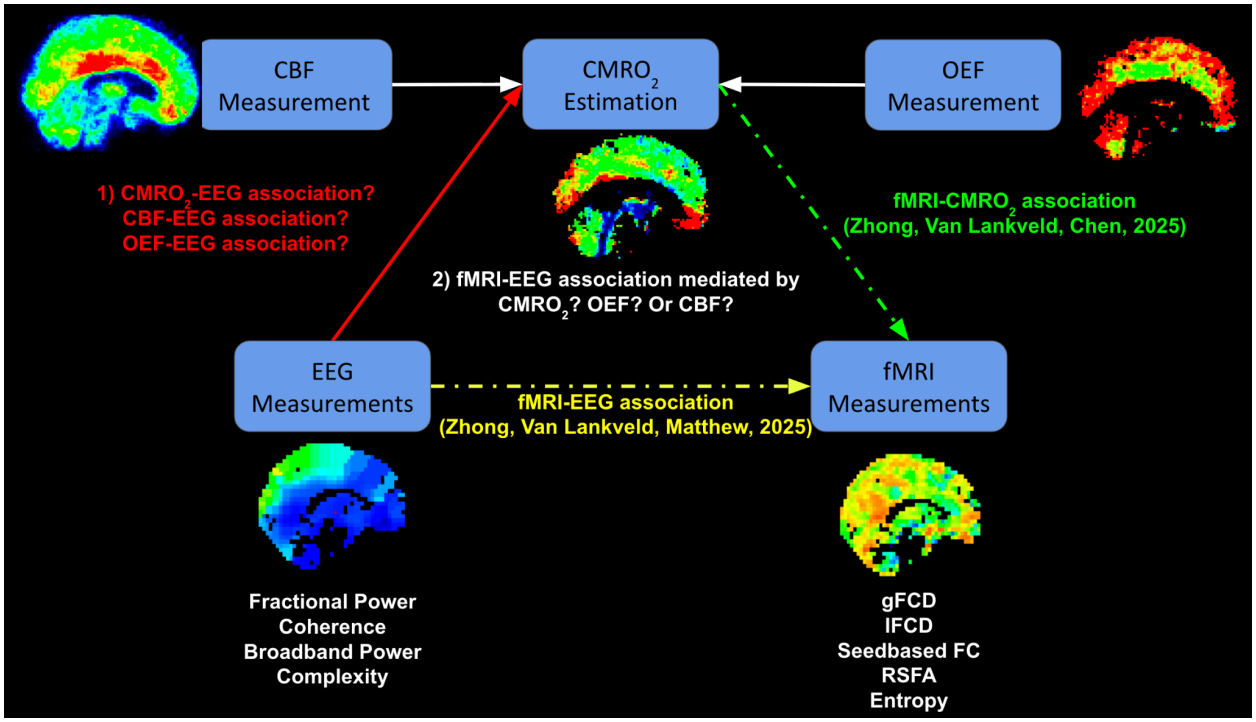

Figure 1. An overview of the analysis framework incorporating the metabolic and electrophysiological associations of rs-fMRI measurements that are tested in this work. In this study, we first examined how EEG measurements are associated with baseline physiological metrics (red arrow). The EEG metrics include bandlimited fractional power, coherence, broadband power, and complexity. The baseline physiological metrics include $CMRO_2$ and its correlates CBF, and OEF (white arrows). We further tested here how $CMRO_2$, CBF, and OEF mediated (the green arrow) the EEG–fMRI association (yellow arrows). The fMRI metrics include gFCD, lFCD, seedbased FC, RSFA and entropy.

2 Method

2.1 Participant

A total of 20 healthy participants are involved in this study (10 M/10 F, age = 20 to 32 years). No participant reported having a history of cardiovascular disease, psychiatric illness, neurological disorder, malignant disease, or medication use that may have affected the study. Participants were recruited through the Baycrest Participants Database. The study was approved by the research ethics board (REB) of Baycrest, and the experiments were performed with written consent from each participant according to REB guidelines.

2.2 MRI Acquisition

The images were acquired using a Siemens Prisma 3 Tesla System (Siemens, Erlangen, Germany), which employed 20-channel phased-array head coil reception and body coil transmission. The participants were imaged during naturalistic-stimulus viewing to reduce random mind-wandering which increases reproducibility (Gal et al., 2022). The following data were acquired for each participant:

1. T1-weighted structural image (sagittal, 234 slices, 0.7 mm isotropic resolution, TE = 2.9 ms, TR = 2240 ms, TI = 1130 ms, flip angle = 10°).
2. Two time-of-flight (TOF) scans, with coronal and sagittal flow encoding, respectively (coronal: 0.8 x 0.8 x 2.125 mm thickness, 100 slices, TR = 16.6 ms, TE = 5.1 ms, flip angle (α) = 60°; sagittal: 0.8 x 0.8 x 2.125 mm thickness, 80 slices, TR = 16.6 ms, TE = 5.1 ms; flip angle (α) = 60°).
3. One dual-echo (DE) pseudo-continuous arterial spin labelling (pCASL) (courtesy of Danny J. J. Wang, University of Southern California) for recording CBF and BOLD dynamics (TR = 4.5 s, TE1 = 9.8 ms, TE2 = 30 ms, post-labelling delay = 1.5 s, labelling duration = 1.5 s, flip angle (α) = 90°, 3.5 mm isotropic resolution, 35 slices, slices gap = 25%, scanning time = 4 minutes), complete with a M_0 scan in which the TR was 10 s and the scan time 45 s, all other parameters remaining the same.
4. One multi-echo gradient echo (MEGRE) scan for static R_2^* mapping (TR = 4 s, TE ranged from 5 ms to 60 ms with the step of 5 ms, flip angle = 20°, magnitude and phase recording, same spatial resolution as the pCASL);
5. One SE MRI data for static R_2 mapping (TR = 10 s, TE =[17, 33, 50, 66, 91, 107, 116] ms, same spatial resolution as the pCASL).

2.3 EEG Acquisition

In a separate session from the MRI, a 256-channel Geodesic Sensor Net with a Net Amp 400 amplifier (Magstim Inc., Roseville, MN, USA) was used to record 4 minutes of resting EEG. A naturalistic stimulus video, which is the same as that used during fMRI acquisition, was shown to participants in order to reduce random mind wandering. The EEG electrodes were attached following the international standard 10-20 system, and the impedance of each electrode was controlled per the vendor recommendations (lower than 50 kOhm recommended for the saline-based system). The EEG signal was digitized at a sampling frequency of 1,000 Hz, and the amplitude resolution was set to 0.024 µV.

2.4 Macrovascular Correction

The macrovascular correction was performed utilizing a biophysical approach that was developed (Zhong, Polimeni, et al., 2024) and validated (Zhong, Van Lankveld, & Chen, 2025; Zhong, Van Lankveld, Mathew, et al., 2025) in our previous studies. This method was designed to correct macrovascular contributions within and beyond the vasculature, as highlighted in our previous findings (Zhong, Tong, et al., 2024). Since the scan parameters were the same between this study and the previous study (Zhong, Van Lankveld, & Chen, 2025) that applied macrovascular correction, none of the parameters in the correction pipeline had been modified.

A summary of the macrovascular correction pipeline is provided below: 1) generate a vascular mask for each participant and estimate the macrovascular blood-volume fraction (fBV); 2) identified the prototypical venous signal fluctuation from the in-vivo BOLD signal from the voxel with the maximum fBV, which was then demeaned and normalized by its maximum (this signal can be assumed to be driven primarily by T_2 fluctuations that mimic the variation in venous blood oxygenation, and can also be assumed to contain little information on localized neuronal activity (Zhong, Polimeni, et al., 2024)); 3) simulate macrovascular BOLD signals using our macro-VAN (vascular anatomical network) model; 4) assess the lag between the simulated signal and the in-vivo signal for each voxel (lag that leads to maximum absolute cross-correlation coefficient); 5) regress the simulated signal from the in-vivo signal for each voxel as nuisance regressor (linear regression model).

2.5 fMRI Preprocessing and Analysis

Two pipelines were used to process the rs-fMRI data: one for investigating seed-based FC and the other for seed-independent measures. In both pipelines, the first five volumes of BOLD data were rejected to allow the BOLD signal to enter steady state. All rs-fMRI metrics were calculated after macrovascular correction. Moreover, all metrics below were averaged within each functional network listed in the *Seed-based rs-fMRI analysis* subsection to calculate network-wise metrics.

2.5.1 Seed-based rs-fMRI analysis

rs-fMRI FC analysis was conducted using the CONN toolbox (Whitfield-Gabrieli & Nieto-Castanon, 2012) with the default_MNI preprocessed pipeline (bandpass filter: 0.01-0.1 Hz; regressed confounds: white matter, CSF and estimated participant-motion parameters). The networks of interest include the visual network (VN), sensorimotor network (SMN), the default mode network (DMN), the language network (LN), the salience network (SN), the dorsal attention network (DAN), and the frontoparietal network (FPN). The seeds for each network were based on the default seed locations provided in the CONN toolbox. To define each network, given the multiple seeds involved, the correlation maps associated individual seeds, thresholded at to $p < 0.0001$ (FDR corrected), were combined to generate the final network definition.

2.5.2 Seed-independent rs-fMRI analysis

As assessing connectivity based on the seed-based connectivity-defined network boundaries may be somewhat circular, multiple seed-independent approaches have been included. rs-fMRI preprocessing pipeline was implemented with customized procedures based on tools from FSL (Jenkinson et al., 2012), AFNI (Cox, 1996) and FreeSurfer (Fischl, 2012). The following steps were included in the preprocessing steps: (a) 3D motion correction (FSL MCFLIRT), (b) slice-timing correction (FSL slicetimer), (c) brain extraction (FSL bet2 and FreeSurfer mri_watershed), (d) rigid body coregistration of functional data to the individual T1 image (FSL FLIRT), (e) regression of the mean signals from white-matter (WM) and cerebrospinal fluid (CSF) regions (fsl_glm), (f) bandpass filtering to obtain frequency band 0.01-0.1 Hz (AFNI 3dBandpass), and (g) spatial smoothing with a 6 mm full-width half-maximum (FWHM) Gaussian kernel (FSL fslmaths). Once the BOLD signal had been preprocessed, we computed the following metrics:

1. Resting-state fluctuation amplitude (RSFA), a measure of BOLD signal fluctuation power, calculated as the standard deviation of the BOLD signal normalized by the mean of the BOLD signal. This metric reflects the BOLD signal temporal variability that underlies the connectivity measurement.
2. lFCD, calculated using the AFNI (3dLFCD) (Cox, 1996) with a threshold of 0.6, with the neighbourhood data defined to include the 6 face-touching voxels, as suggested by the previous study (Tomasi & Volkow, 2010). gFCD, calculated using the same threshold value (0.6) but within the entire gray matter (Tomasi & Volkow, 2011). The gFCD and lFCD reflect the number of voxels that each voxel is significantly correlated to (globally or locally). The regions with high gFCD and lFCD have previously been referred to as functional connectivity hubs (Shokri-Kojori et al., 2019; Tomasi & Volkow, 2010, 2011).
3. BOLD signal entropy, calculated as the sample entropy with $m = 3$ and $r = 0.6$ related to the standard deviation as proposed by the previous study (Nezafati et al., 2020). The entropy reflects the brain's capacity for information processing and its adaptability to various cognitive and environmental demands (Z. Wang, 2021) that may not be captured by other linear properties such as gFCD and RSFA.

Since FC density-related measurements follow an exponential distribution, log-transformed lFCD and gCDF were used in subsequent statistical analyses (Shokri-Kojori et al., 2019).

2.6 Baseline Perfusion Estimation

First, the ASL data was skull-stripped, and motion correction was applied to label and control images separately before surround subtraction was performed to determine the signal difference time series. To ensure the brain entered a steady state, the first five volumes of ASL data were also discarded, which is similar to in the rs-fMRI pipeline. The static CBF value was quantified using the BASIL toolbox from FSL (oxford_asl) (Chappell et al., 2009). The static CBF maps were also averaged within each functional network listed in the *Functional Network Delimitation* subsection.

Static fractional CBV will be calculated from static CBF by applying linear regression between regionally-averaged baseline static CBF (as ml/100ml/min) and CBV (as a fraction) values in gray and white matter (Eq. 1), measured by previous research with ^{15}O steady-state inhalation PET in 34 healthy participants (Leenders et al., 1990; Ma et al., 2020; Zhang et al., 2018).

$$CBV = (0.0723CBF + 1.144)/100 \tag{1}$$

2.7 Baseline Metabolism Estimation

Both the SE images and the MEGRE image were first skull-stripped, and then the rigid-body coregistration was performed to align SE and MEGRE images with the T1-weighted image. Using SE images, R_2 (refocusable transverse relaxation rate) values were determined based on a single exponential model fitted to each TE. Since the MEGRE scan is sensitive to background fields, a background field correction was performed on the MEGRE data (Kaczmarz et al., 2020). The corrected MEGRE magnitude images were then fitted using a single exponential model to estimate R_2^*. The R_2' was calculated as the difference between R_2 and R_2^*. The OEF and $CMRO_2$ were estimated using R_2' and perfusion parameters as described in Eq.2 and Eq.3. The theoretical details of metabolism estimation were included in our previous study (Zhong, Van Lankveld, & Chen, 2025). The static OEF and $CMRO_2$ maps were also averaged within each functional network listed in the *Functional Network Delimitation* subsection.

$$OEF = \frac{R_2'}{\frac{4}{3}\pi \times \gamma \times \Delta\chi \times B_0 \times CBV} \tag{2}$$

where R_2' is estimated from R_2 and R_2*, which reflects MR signal dephasing resulting from local magnetic field inhomogeneities. γ is the proton gyromagnetic ratio, and $\Delta\chi$ is the susceptibility difference between oxygenated and deoxygenated blood, CBV is cerebral blood volume, and its estimation will be described in the Baseline perfusion estimation section. OEF was restricted to be between 0 and 1. Using the OEF estimate, quantitative $CMRO_2$ can then be estimated (Göttler et al., 2019) as follows,

$$CMRO_2 = CaO_2 \times CBF \times OEF \tag{2}$$

where CaO_2 is the arterial oxygen content, set to $19\ ml\ O_2/100\ ml\ blood$ (An et al., 2001).

2.8 EEG preprocessing and analysis

2.8.1 Preprocessing

EEG preprocessing was carried out using EEGLAB (version 2019.1) (Delorme & Makeig, 2004) with functions implemented in Matlab (The MathWorks Inc., Natick, Massachusetts, USA). The following steps were included in the preprocessing pipeline: 1) removal of face electrodes; 2) downsampling to 125 Hz; 3) high-pass filtering with a cut-off frequency of 1 Hz; 4) ICA denoising (removal of components related to physiological sources, including eye blinks, eye movements, residual ballistocardiograph artifacts and muscle activity); 5) channel rejection (criteria: more than 80% noisy data, line noise exceeding 4 standard deviations, flat-line segments of more than 5 seconds); 6) linear detrending.

The source reconstruction was performed using the Cartool toolbox (version 4.11) (Brunet et al., 2011). The forward model was developed for each participant using the T1-weighted MRI scans and the Locally Spherical Model with Anatomical Constraints (LSMAC) model (6-shell). The thickness and conductivity of the skull were adjusted according to each participant's age. The inverse model was estimated using exact low-resolution brain electromagnetic tomography (eLORETA) (Imperatori et al., 2020) with 6000 solution points. The dominant orientation of the source signal was determined using singular-value decomposition (SVD) of each voxel. In addition, the sources were further mapped back to the fMRI space based on coordinates with the nearest neighbour principle so that the following metrics could be averaged with the same network ROIs as the fMRI metrics.

2.8.2 EEG power

The Fourier transform was applied to the signal from each source. Band-specific fractional power was determined by dividing the power of each band by the total power across all bands, with bands defined as follows: delta (1-4 Hz), theta (4-8 Hz), alpha (8-12 Hz), beta (12-30 Hz) and low gamma (30-50 Hz). This is the same definition of bands as used in our previous study (Zhong & Chen, 2022). Unlike raw band-limited power, normalized power accounts for fluctuations in total power while quantifying the contribution of each band. Additionally, the total power across all bands was normalized by the spatial standard deviation of the total power for each participant to account for different SNRs across participants.

2.8.3 EEG coherence

The imaginary part of EEG-signal coherence has been widely used to measure synchronization between two EEG signals, since it is less sensitive to volume conduction effects (Nolte et al., 2004). Our study utilized this approach to quantify EEG-based brain connectivity (Nentwich et al., 2020; Nolte et al., 2004) with a frequency resolution of 0.5 Hz and an overlap of 0.5 using scripts adapted from the Brainstorm toolbox (Tadel et al., 2011). Band-limited coherence for each band was calculated by averaging the coherence spectrum over the frequency range of each band as defined earlier. Moreover, total coherence was calculated by averaging the coherence spectrum across all bands. Here, band-limited coherence reflects functionally specific connectivity, whereas broadband coherence reflects coordination across different neuronal processes across bands.

The imaginary coherence was calculated as follows. First, we computed the cross-spectrum between the two signals, S_{uv}

$$S_{UV} = \frac{1}{N}\sum_{n=1}^{N} U_n(f)V_n^*(f) \quad (4)$$

where N refers to the number of samples in the time course, and U and V refer to the Fourier transform of the two signals, respectively.

$$Coh = \frac{S_{UV}}{\sqrt{S_{UU}(f)S_{VV}(f)}} \quad (5)$$

The complex coherence of the signal was calculated as the cross-spectrum normalized by their auto-spectra. Imaginary coherence is the magnitude of the imaginary part of the complex coherence.

2.8.4 EEG complexity index (CI)

The complexity index was calculated as in our previous study (Zhong & Chen, 2022). The order of permutation was set to 2 and the noise threshold was 0.5 relative to the standard deviation of each band, while the scales were chosen as 3, 6, 13, 21 and 62 to represent coarse to fine temporal components of the signal. The sample entropy was used to calculate the entropy for each scale. The complexity index (CI) was calculated using the area under the multiscale entropy curve.

2.9 Analysis of Metabolic and Electrophysiological Underpinnings of rs-fMRI

2.9.1 Analysis of associations between $CMRO_2$ and EEG metrics

The associations between network-averaged metabolism and hemodynamics as well as EEG metrics were assessed using a linear mixed-effects model (LME) approach. As in our previous study (Zhong, Van Lankveld, & Chen, 2025), sex was also included as a fixed effect, since sex effects have been observed in both metabolism and hemodynamics (Aanerud et al., 2017) EEG metrics (Nentwich et al., 2020; Zhong & Chen, 2022). The z-transform was applied to all parameters prior to model fitting. Outliers were detected and removed for each fitting according to the 1.5 interquartile range (IQR) criterion. An overview of the parameters of interest is presented in **Table 1** and the model (across all networks and all participants, 140 data points in total) is described as Eq. 3. A significance level of 0.05 was used with a false discovery rate (FDR).

Table 1. Parameters for linear mixed-effects model.

Y ~ 1 + X + Sex + X:Sex (Eq. 2)	
Y (EEG)	X (Metabolism and Hemodynamics)
Coherence (Broadband)	$CMRO_2$
Coherence (Band-limited)	CBF
CI	OEF

fractional power (Band-limited)	
Total power (Broadband)	

2.9.2 Mediation analysis

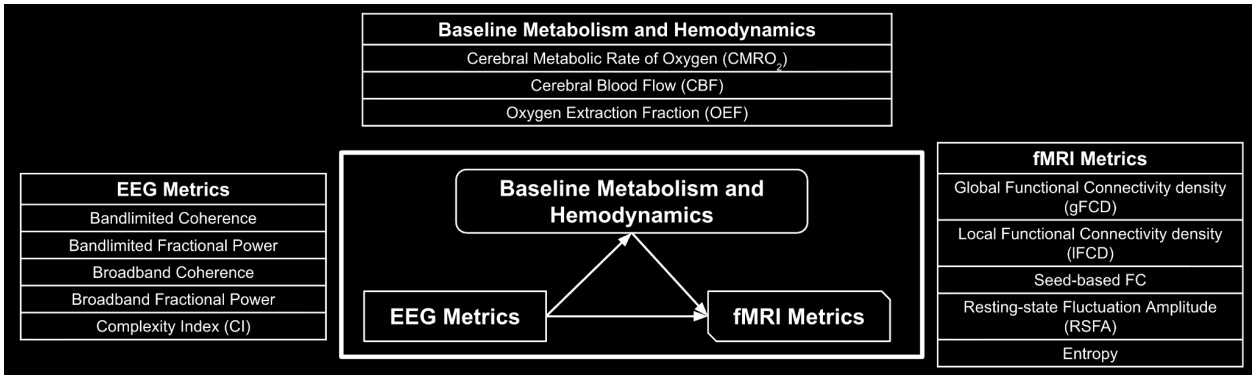

Figure 2. Demonstration of the meditation analysis. EEG–fMRI associations were tested for mediation by metabolic and hemodynamic metrics ($CMRO_2$, CBF, or OEF).

Mediation analysis (**FIg. 2**) was conducted using triplets of EEG, rs-fMRI, and baseline metabolic and hemodynamic variables, considering only significant three-way associations. Prior to the analysis, the effect of sex was regressed out from all metrics. Models were implemented in MATLAB using Variational Bayesian Analysis (VBA) (Daunizeau et al., 2014) following the three-step mediation procedure of Baron and Kenny (Baron & Kenny, 1986). To assess whether the inclusion of the mediator significantly reduced the association between the independent and dependent variables (EEG to fMRI metrics), the Sobel test was applied, with significance set at $p < 0.05$ (Sobel, 1982). Results were classified as showing full mediation, partial mediation, or no mediation.

3 Results

3.1 Metabolic and Hemodynamic Associations of Band-limited EEG Metrics

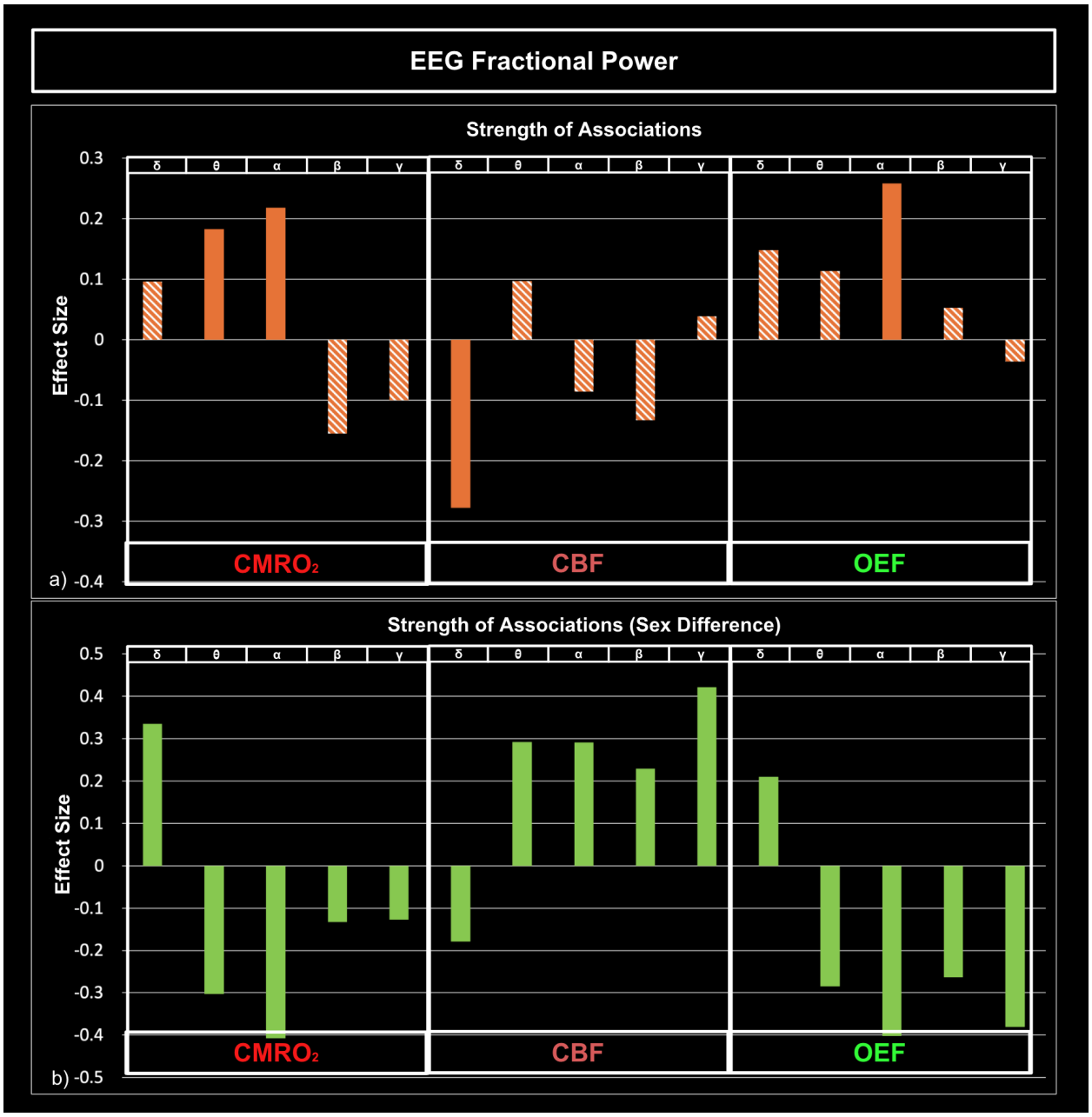

Figure 3. Associations between baseline metabolic and hemodynamic variables ($CMRO_2$, CBF and OEF) and EEG band-limited fractional power. a) Strength of associations between rs-fMRI metrics and EEG band-limited fractional power; b) comparison of the strength of associations between males and females, with a positive effect

size indicating a stronger association in males. Solid bars: association with statistical significance; striped bars: association with no statistical significance.

EEG band-limited fractional power was associated with baseline metabolic and hemodynamic variables, though only to a limited extent (**FIg. 3a**). Significant positive correlations were observed between $CMRO_2$ and the fractional power in theta and alpha bands, while the delta band fractional power was negatively associated with OEF. Additionally, CBF showed a significant positive association with alpha band fractional power. Notably, none of the metabolic or hemodynamic metrics were significantly associated with the beta or gamma band fractional power.

Significant sex interaction effects were also observed between EEG fractional power and baseline metabolic and hemodynamic variables (**FIg. 3b**). For the delta band, associations with $CMRO_2$ were stronger in males, whereas associations with OEF and CBF were stronger in females. In the other frequency bands, sex interactions showed opposite patterns: females exhibited stronger associations with $CMRO_2$, while males showed stronger associations with OEF and CBF. Interestingly, although many frequency bands exhibited significant sex interaction effects, some of these associations were not statistically significant. The detailed statistics are included as **Table. S1**.

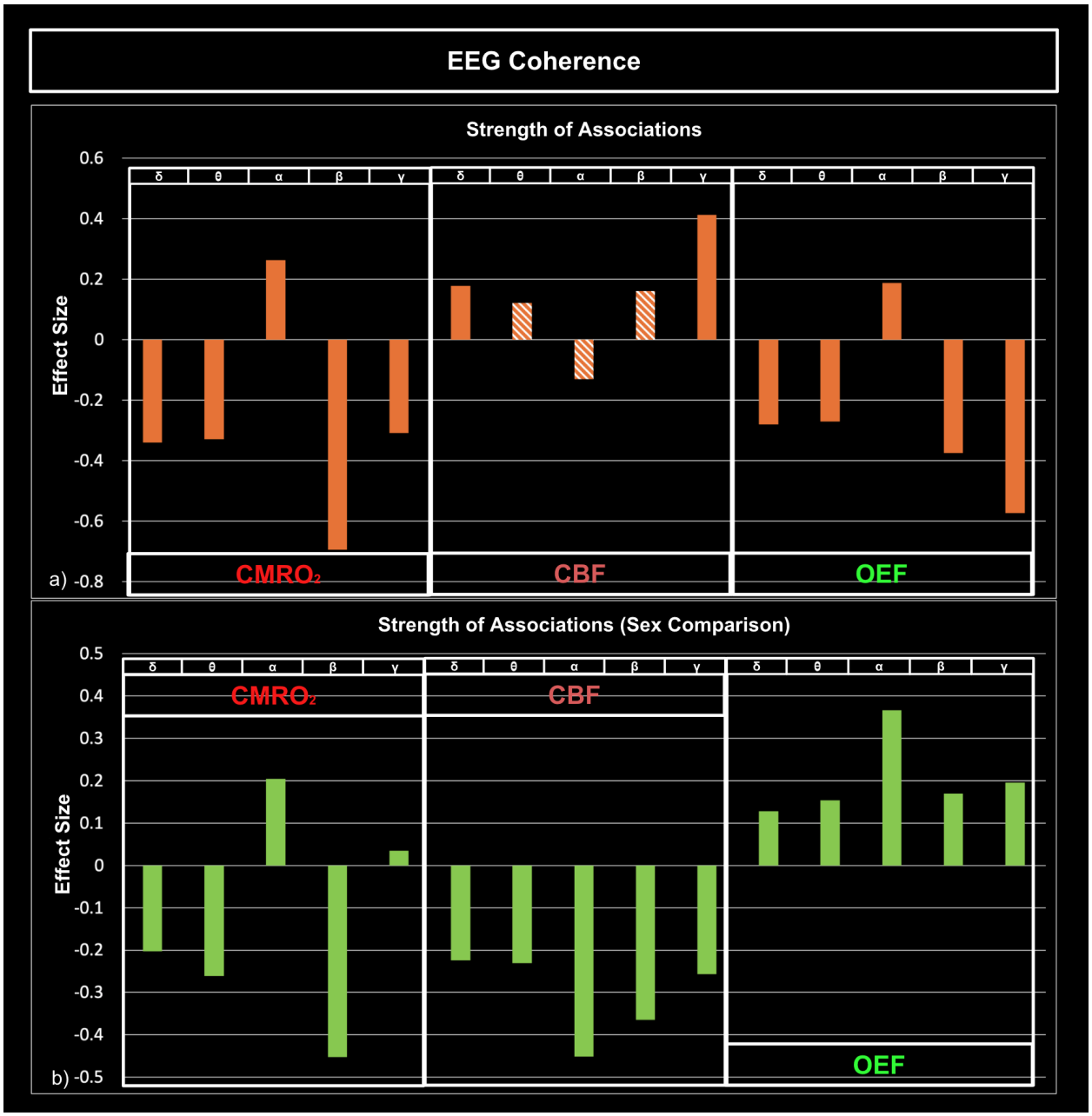

Figure 4. Associations between baseline metabolic and hemodynamic variables ($CMRO_2$, OEF, CBF) and EEG band-limited coherence. a) Strength of associations between rs-fMRI metrics and EEG band-limited coherence; b) comparison of strength of associations between males and females, with a positive effect size indicating a stronger association in males. Solid bars: association with statistical significance; striped bars: association with no statistical significance.

$CMRO_2$ and CBF were extensively associated with EEG band-limited coherences, whereas few significant associations were observed for OEF (**FIg. 4a**). Specifically, $CMRO_2$ and CBF showed significant negative associations with delta, theta, beta, and gamma coherences, while their association with alpha coherence was significantly positive. OEF was significantly positively associated only with delta and gamma band coherences.

Similar to band-limited fractional power, significant sex interaction effects were observed in the associations of EEG band-limited coherences (**FIg. 4b**). For $CMRO_2$, females exhibited stronger associations with delta, theta, and beta coherences, whereas males showed stronger associations with alpha coherence. Females also showed stronger associations between OEF and EEG coherences across all frequency bands. In contrast, males demonstrated stronger associations between CBF and EEG coherences across all frequency bands except for the beta band. The detailed statistics are included in **Table S2**.

3.2 Metabolic and Hemodynamic Associations of Broadband EEG Metrics

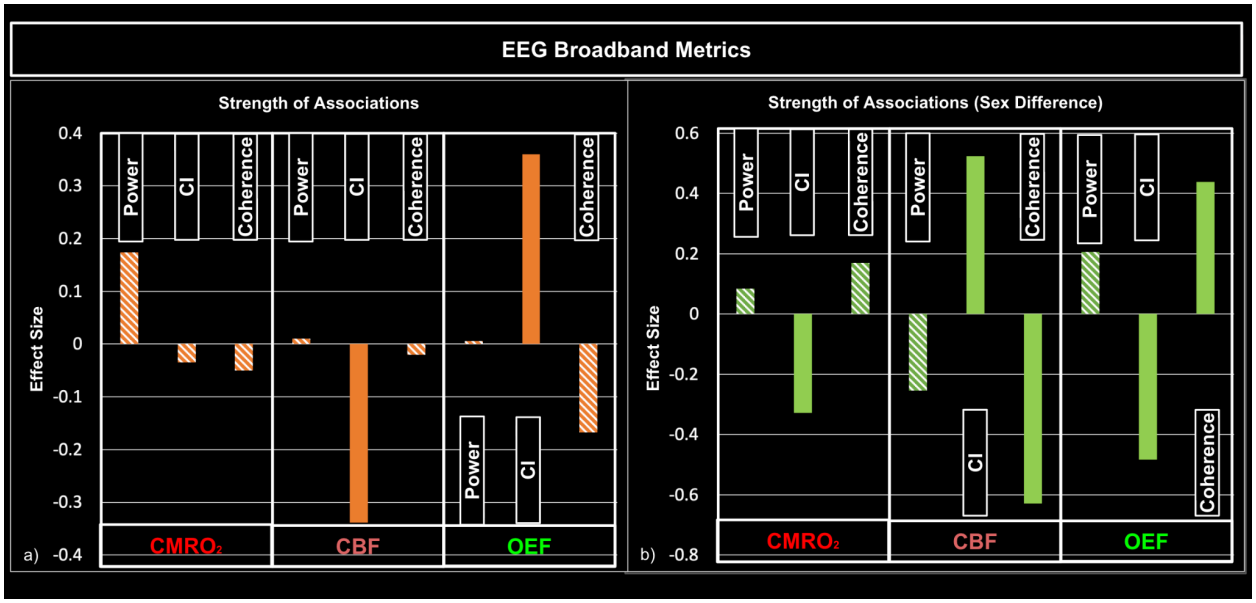

Figure A. Associations between baseline metabolic and hemodynamic variables (OEF, CBF and $CMRO_2$) and EEG broadband metrics. a) Strength of associations between rs-fMRI metrics and EEG band-limited broadband metrics; b) comparison of strength of associations between males and females, with a positive effect size indicating a stronger association in males. Solid bars: association with statistical significance; striped bars: association with no statistical significance.

Metabolic and hemodynamic variables were closely associated with some, but not all, EEG broadband metrics (**FIg. 5a**). Associations were primarily observed with band-limited EEG CI, but not with power and coherence. EEG CI was negatively associated with OEF and positively associated with CBF.

Significant sex interaction effects were also observed (**FIg. 5b**). Females showed stronger associations with $CMRO_2$ and EEG CI. CBF in females was more strongly associated with EEG CI, while in males CBF was more strongly associated with EEG coherence. Opposite to CBF, for OEF, females were more strongly associated with coherence, while males were more strongly associated with CI. The detailed statistics are included in **Table S3**.

3.3 The Role of Metabolism and Hemodynamics in Mediating EEG and fMRI Associations

In this work CMRO2 was found to mediate the association between the following EEG and fMRI metrics:

- EEG power ratio: theta to lFCD (partial, ab = 0.39, p = 0.015).
- EEG coherence: delta to gFCD (full, ab = -2.66 p = 0.002); theta to gFCD (full, ab = -5.38, p = 0.009); beta to gFCD (partial, ab = -3.02, p = 0.003); beta to lFCD (full, ab = -0.58, p = 0.023); gamma to gFCD (partial, ab = -6.31, p = 0.002).

Moreover, CBF and OEF was found to mediate the association between the following EEG and fMRI metrics:

- Mediation by OEF:
    - EEG power ratio: none.
    - EEG coherence: gamma to seed-based FC (full, ab = -1.38, p = 0.011).
- Mediation by CBF:
    - EEG power ratio: None.
    - EEG coherence: beta to gFCD (partial, ab=-2.88, p=0.005); gamma to lFCD (partial, ab = 2.83, p = 0.021)

4 Discussion

Understanding how EEG and $CMRO_2$ underlie rs-fMRI metrics provides a stronger foundation for interpreting rs-fMRI findings. The main findings are:

1. Band-limited fractional power was significantly associated with baseline metabolic and hemodynamic variables in all EEG bands except the beta band.

    a. Positive for $CMRO_2$ and CBF
    b. Negative for OEF
2. Band-limited coherences were significantly associated with baseline metabolic and hemodynamic variables in all EEG bands except the beta band.
    a. Positive for OEF as well as CBF-beta and $CMRO_2$-beta
    b. Negative for the CBF and $CMRO_2$ with the rest of the frequency bands
3. EEG broadband power and complex index (CI) were positively associated with $CMRO_2$, while coherence was negatively associated with OEF.
4. Significant sex dependence was found for all of the above associations.
5. The baseline metabolic and hemodynamic associations with EEG significantly modulated some of the EEG-fMRI associations, primarily manifesting through $CMRO_2$ but minimally through CBF.

4.1 The association between EEG and $CMRO_2$

The association between EEG and $CMRO_2$ has long been assumed (Attwell & Laughlin, 2001), yet direct evidence or quantitative assessment of this relationship has been lacking. In this study, we demonstrate how EEG fractional power and coherence (connectivity) relate to metabolic and hemodynamic measures, revealing that these associations are highly dependent on EEG oscillation frequency and differ across

EEG metrics. Interestingly, nearly all networks exhibited the same polarity of association as the whole-brain results, suggesting that these associations are primarily driven by inter-participant variability rather than inter-regional variability. The physiological basis for why the EEG–$CMRO_2$ association primarily emerges at the inter-participant level, even among healthy young adults, presents an intriguing question for future research.

4.1.1 Band-limited Fractional Power

Fractional power has been used to reflect the strength of locally synchronized EEG activity, with stronger synchronization thought to require greater energy supply (Y. Wang et al., 2017). While this holds true in general, it does not apply uniformly across all EEG frequency bands. For low-frequency oscillations (theta and alpha), we observed clear positive associations between EEG fractional power and $CMRO_2$ (**Fig. 3**), suggesting that increased local synchronization is accompanied by greater oxidative metabolism. In contrast, high-frequency power (beta and gamma) were not significantly associated with static $CMRO_2$). To the best of our knowledge, only two studies (Buchan et al., 1997; Nagata et al., 1989) have examined the association between EEG band power and $CMRO_2$ directly (rather than with $CMRO_2$ surrogates such as CBF or $CMRO_{glu}$), and both reported negative $CMRO_2$ associations for EEG power below 8 Hz (delta and theta) and positive associations for power above 8 Hz (alpha and beta). However, both studies focused on patient populations (Alzheimer's disease and cerebral infarction, respectively) rather than healthy participants. Thus, we have no healthy-adult literature as reference, suggesting that these associations may differ across physiological conditions, as also indicated by previous findings (Buchan et al., 1997). This further highlights the potential of such associations as biomarkers for neurological conditions such as Alzheimer’s disease (Buchan et al., 1997).

4.1.2 Band-limited Coherence

We found that only alpha coherence was positively associated with $CMRO_2$, consistent with our EEG–fMRI findings, where alpha was the only frequency band in which coherence was positively associated with gFCD (Zhong, Van Lankveld, Mathew, et al., 2025), which is in turn strongly associated with $CMRO_2$ (Zhong, Van Lankveld, & Chen, 2025). This suggests that alpha coherence may dominate large-scale connectivity patterns, as discussed in our previous studies (Zhong, Van Lankveld, Mathew, et al., 2025). Unlike the complex EEG–OEF and EEG–CBF relationships observed for fractional power, the EEG–$CMRO_2$ association for coherence was fully explained by the EEG–OEF association, suggesting that a higher CBF might not be required to sustain a high degree of large-scale electrophysiological synchronization.

4.1.3 Broadband EEG

Although $CMRO_2$ is expected to reflect the overall rate of oxygen consumption across total neural activity rather than for band-specific activity, different EEG bands are likely to exhibit different metabolic profiles. Specifically, high-frequency EEG activity can reflect aerobic glycolysis (Theriault et al., 2023), which is independent from $CMRO_2$, but broadband EEG metrics might still be predominantly driven by low-frequency activity (the 1/f effect) (Gyurkovics et al., 2021). Thus, a positive association between EEG broadband power and $CMRO_2$ is expected. However, we did not observe significant association between broadband EEG power and $CMRO_2$ after FDR correction (although a positive association was observable before FDR correction, $p = 0.04$), suggesting there might be a considerable role for aerobic glycolysis more broadly

(**Fig. RC**). We also observed a negative CI–CBF association and a positive CI–OEF association, although the underlying mechanisms remain unclear given the complex, non-linear characteristics of CI.

4.3 Sex Effect on EEG-$CMRO_2$ Association

In theory, the EEG-$CMRO_2$ associations can be explained by either EEG-CBF associations or EEG-OEF associations. For example, the positive alpha EEG–$CMRO_2$ association was accompanied by a positive EEG–OEF association without a significant EEG–CBF association. This finding diverges from prior assumptions and from task-based fMRI models, which link metabolic demand with CBF (Buxton et al., 1998; Zhong, Van Lankveld, Mathew, et al., 2025). Nonetheless, given that our findings are based on inter-subject variations in static resting-state physiological metrics, the comparability with task contrasts is unclear, especially if the inter-subject variations are strongly driven by sex.

Interestingly, the EEG–$CMRO_2$ association also exhibits a pronounced sex dependence. Notably, females showed stronger EEG–$CMRO_2$ and EEG–OEF associations (except for in the delta band), whereas males exhibited stronger EEG–CBF associations. These findings suggest sex differences in energy utilization patterns, potentially linked to higher aerobic glycolysis and CBF in females (Aanerud et al., 2017; Gur & Gur, 1990; Rettberg et al., 2014). In this scenario, increased neural activity that is measurable by EEG in females may shift energy metabolism from aerobic glycolysis toward oxidative phosphorylation, leading to increased OEF and $CMRO_2$. Given the characteristically higher baseline CBF in females, as discussed earlier, an inter-subject association between $CMRO_2$ and CBF in females may not exist to the same extent as in males. Although the delta band displayed the opposite trends as the other bands in terms of sex dependence, this may relate to its inhibitory role in neural processing. Further research is needed to disentangle these sex-dependent effects.

Strong sex-dependent effects were also observed in the associations between $CMRO_2$ and EEG coherence. Similar to the case of EEG fractional power, females showed stronger associations across all frequency bands except the alpha band. This pattern may reflect a shift from aerobic glycolysis to oxidative metabolism, as discussed for fractional power. Interestingly, the sex dependencies of EEG–CBF and EEG–OEF associations differed from those observed for EEG fractional power and, in some cases, the directionalities were even reversed. For instance, females exhibited stronger EEG–CBF but weaker EEG–OEF associations. This divergence may arise from connectivity and power are two dimensions of brain activity.

Unlike in the case of the band-limited metrics, the sex effects for power–CBF/OEF and coherence–CBF/OEF associations were more modest. Specifically, EEG CI was the only metric manifesting significant associations with CBF and OEF and significant sex differences in these associations. This may reflect fundamental differences in the underlying interpretations of broadband (Brake et al., 2024; Férat et al., 2022), potentially in the lack of specificity in the interpretation of broadband EEG metrics. Nonetheless, the fact that we observed consistent sex differences in both bandlimited and broadband EEG metrics highlights the importance of incorporating sex differences in investigating the neurometabolic origins of rs-fMRI.

4.4 Metabolism and Hemodynamics Partially Mediate the EEG–fMRI Associations

The ultimate motivation for this work is to better understand the neuronal underpinnings of rs-fMRI. As discussed in our previous studies (Zhong, Van Lankveld, & Chen, 2025; Zhong, Van Lankveld, Mathew, et al., 2025), the current understanding is that the association between EEG and fMRI is indirect and likely mediated, at least in part, by $CMRO_2$. Indeed, our results suggest that $CMRO_2$ significantly mediates the EEG–fMRI association, primarily for gFCD and lFCD. Other metrics, such as RSFA and seed-based FC did not manifest strong EEG associations across the group. Moreover, limited mediation was observed for CBF and OEF. This is interesting given that $CMRO_2$ is mathematically related to OEF and CBF (Göttler et al., 2019; Zhong, Van Lankveld, & Chen, 2025), and suggests that $CMRO_2$ confers unique variance not accounted for by CBF and OEF. Therefore, caution is warranted when using CBF as a surrogate for $CMRO_2$ across participants. However, these mediations by $CMRO_2$ will likely not fully explain the mechanism linking EEG and fMRI. The lack of significant CBF mediation further suggests that the CBF-$CMRO_2$ coupling in a static resting state context is likely different than during task-related activity.

The basis of neurovascular coupling has long been debated. Increasingly, it is becoming recognized that neural activity can influence hemodynamics through multiple mechanisms independent of $CMRO_2$ (e.g., nitric oxide signaling) (Drew, 2022). Additionally, the autonomic nervous system can modulate both EEG and fMRI signals to varying extents independently of $CMRO_2$ (Bolt et al., 2025; Chalas et al., 2025), even outside brain regions directly responsible for autonomic activity. Moreover, recent insights into the role of aerobic glycolysis in brain metabolism highlight that EEG activity—particularly at higher frequencies—may not be directly linked to $CMRO_2$ (Theriault et al., 2023; Vaishnavi et al., 2010). However, because these high-frequency activities are strongly associated with fMRI signals (Lachaux et al., 2007), they suggest the presence of an EEG–fMRI association pathway that might not be fully mediated by $CMRO_2$ (Tu et al., 2024).

4.5 Limitations

This study unavoidably cannot be free from limitations. Limitations and concerns directly related to the macrovascular correction, mainly involving limitations in TOF imaging acquisition and marco-VAN model simulation, have already been addressed in our previous paper (Zhong, Polimeni, et al., 2024; Zhong, Tong, et al., 2024; Zhong, Van Lankveld, & Chen, 2025; Zhong, Van Lankveld, Mathew, et al., 2025) and will not be repeated here.

Moreover, a limitation of this study is that data from the three modalities were not recorded simultaneously. As a result, we had to assume that the static properties of neuronal activity remained comparable between the EEG and rs-fMRI sessions for each participant. Thus, we used a naturalistic resting-state paradigm, presenting synchronized video content across sessions to help ensure similar brain states across modalities. Additionally, the study included a modest number of participants due to the challenges of multimodal data acquisition. Another limitation is that oxidative metabolism was not directly measured; rather, it was inferred from CBF and OEF measurements, making our $CMRO_2$ estimates inherently dependent on CBF. Nonetheless, this constraint is shared by many MRI- and positron emission tomography (PET)-based (Kudomi et al., 2013) approaches and remains difficult to circumvent. Finally, while we interpret the observed associations in physiological terms, they are derived from statistical associations and do not necessarily reflect causal or mechanistic relationships,

particularly regarding the $CMRO_2$ mediation. This is a broader challenge faced by physiological MRI in general. Future studies with direct, simultaneous measurements across modalities in diverse physiological conditions are essential to establish the underlying biophysical basis of rs-fMRI from multiple perspectives.

5 Conclusion

Despite the widespread use of rs-fMRI, its biophysiological basis remains poorly understood. Building on our previous work, we examined how EEG metrics relate to baseline metabolism ($CMRO_2$ and OEF) and hemodynamics (CBF), and further tested how EEG–$CMRO_2$ associations, together with fMRI–$CMRO_2$ associations, mediate the EEG–fMRI relationship. We established associations between EEG and $CMRO_2$ and found that $CMRO_2$ only partially mediates the EEG–fMRI relationship. We also uncovered substantial sex-related differences in these associations. This study provides new insight into how electrophysiological, metabolic, and rs-fMRI measures are interconnected, advancing our understanding of both rs-fMRI and cerebral physiology.

Acknowledgement

The authors would like to acknowledge financial support from Canadian Institutes of Health Research and the Canada Research Chairs Program (JJC) and funding support from Ydessa Hendeles Graduate Scholarship (XZZ).

References

Aanerud, J., Borghammer, P., Rodell, A., Jónsdottir, K. Y., & Gjedde, A. (2017). Sex differences of human cortical blood flow and energy metabolism. *Journal of Cerebral Blood Flow and Metabolism: Official Journal of the International Society of Cerebral Blood Flow and Metabolism*, *37*(7), 2433–2440. https://doi.org/10.1177/0271678X16668536

Andreason, P. J., Zametkin, A. J., Guo, A. C., Baldwin, P., & Cohen, R. M. (1994). Gender-related differences in regional cerebral glucose metabolism in normal volunteers. *Psychiatry Research*, *51*(2), 175–183. https://doi.org/10.1016/0165-1781(94)90037-x

An, H., Lin, W., Celik, A., & Lee, Y. Z. (2001). Quantitative measurements of cerebral metabolic rate of oxygen utilization using MRI: a volunteer study. *NMR in Biomedicine*, *14*(7-8), 441–447. https://doi.org/10.1002/nbm.717

Attwell, D., & Laughlin, S. B. (2001). An energy budget for signaling in the grey matter of the brain. *Journal of Cerebral Blood Flow and Metabolism: Official Journal of the International Society of Cerebral Blood Flow and Metabolism*, *21*(10), 1133–1145. https://doi.org/10.1097/00004647-200110000-00001

Baron, R. M., & Kenny, D. A. (1986). The moderator–mediator variable distinction in social psychological research: Conceptual, strategic, and statistical considerations. *Journal of Personality and Social Psychology*, *51*(6), 1173–1182. https://doi.org/10.1037/0022-3514.51.6.1173

Biswal, B., Yetkin, F. Z., Haughton, V. M., & Hyde, J. S. (1995). Functional connectivity in the motor cortex of resting human brain using echo-planar MRI. *Magnetic Resonance in Medicine*, *34*(4), 537–541. https://doi.org/10.1002/mrm.1910340409

Bolt, T., Wang, S., Nomi, J. S., Setton, R., Gold, B. P., deB Frederick, B., Yeo, B. T. T., Chen, J. J., Picchioni, D., Duyn, J. H., Spreng, R. N., Keilholz, S. D., Uddin, L. Q., & Chang, C. (2025). Autonomic physiological coupling of the global fMRI signal. *Nature Neuroscience*, *28*(6), 1327–1335. https://doi.org/10.1038/s41593-025-01945-y

Brake, N., Duc, F., Rokos, A., Arseneau, F., Shahiri, S., Khadra, A., & Plourde, G. (2024). A neurophysiological basis for aperiodic EEG and the background spectral trend. *Nature Communications*, *15*(1), 1514. https://doi.org/10.1038/s41467-024-45922-8

Brunet, D., Murray, M. M., & Michel, C. M. (2011). Spatiotemporal analysis of multichannel EEG: CARTOOL. *Computational Intelligence and Neuroscience*, *2011*, 813870. https://doi.org/10.1155/2011/813870

Buchan, R. J., Nagata, K., Yokoyama, E., Langman, P., Yuya, H., Hirata, Y., Hatazawa, J., & Kanno, I. (1997). Regional correlations between the EEG and oxygen metabolism in dementia of Alzheimer's type. *Electroencephalography and Clinical Neurophysiology*, *103*(3), 409–417. https://doi.org/10.1016/s0013-4694(97)00015-5

Buxton, R. B., Wong, E. C., & Frank, L. R. (1998). Dynamics of blood flow and oxygenation changes during brain activation: the balloon model. *Magnetic Resonance in Medicine*, *39*(6), 855–864. https://doi.org/10.1002/mrm.1910390602

Chalas, N., Saltafossi, M., Berther, T., Balestrieri, E., Abbasi, O., Gross, J., & Kluger, D. S. (2025). Respiration as a dynamic modulator of sensory sampling. In *bioRxiv*. https://doi.org/10.1101/2025.06.26.661828

Chappell, M. A., Groves, A. R., Whitcher, B., & Woolrich, M. W. (2009). Variational Bayesian inference for a nonlinear forward model. *IEEE Transactions on Signal Processing: A Publication of the IEEE Signal Processing Society*, *57*(1), 223–236. https://doi.org/10.1109/tsp.2008.2005752

Cholet, N., Seylaz, J., Lacombe, P., & Bonvento, G. (1997). Local uncoupling of the cerebrovascular and metabolic responses to somatosensory stimulation after neuronal nitric oxide synthase inhibition. *Journal of Cerebral Blood Flow and Metabolism: Official Journal of the International Society of Cerebral Blood Flow and Metabolism*, *17*(11), 1191–1201. https://doi.org/10.1097/00004647-199711000-00008

Corsi-Cabrera, M., Ramos, J., Guevara, M. A., Arce, C., & Gutiérrez, S. (1993). Gender differences in the EEG during cognitive activity. *The International Journal of Neuroscience*, *72*(3-4), 257–264. https://doi.org/10.3109/00207459309024114

Cox, R. W. (1996). AFNI: software for analysis and visualization of functional magnetic resonance neuroimages. *Computers and Biomedical Research, an International Journal*, *29*(3), 162–173. https://doi.org/10.1006/cbmr.1996.0014

Daunizeau, J., Adam, V., & Rigoux, L. (2014). VBA: a probabilistic treatment of nonlinear models for neurobiological and behavioural data. *PLoS Computational Biology*, *10*(1), e1003441. https://doi.org/10.1371/journal.pcbi.1003441

Delorme, A., & Makeig, S. (2004). EEGLAB: an open source toolbox for analysis of single-trial EEG

dynamics including independent component analysis. *Journal of Neuroscience Methods*, *134*(1), 9–21. https://doi.org/10.1016/j.jneumeth.2003.10.009

Drew, P. J. (2022). Neurovascular coupling: motive unknown. *Trends in Neurosciences*, *45*(11), 809–819. https://doi.org/10.1016/j.tins.2022.08.004

Duffy, F. H., Mcanulty, G. B., & Albert, M. S. (1996). Effects of age upon interhemispheric EEG coherence in normal adults. *Neurobiology of Aging*, *17*(4), 587–599. https://doi.org/10.1016/0197-4580(96)00007-3

Férat, V., Seeber, M., Michel, C. M., & Ros, T. (2022). Beyond broadband: Towards a spectral decomposition of electroencephalography microstates. *Human Brain Mapping*, *43*(10), 3047–3061. https://doi.org/10.1002/hbm.25834

Fischl, B. (2012). FreeSurfer. *NeuroImage*, *62*(2), 774–781. https://doi.org/10.1016/j.neuroimage.2012.01.021

Gal, S., Coldham, Y., Tik, N., Bernstein-Eliav, M., & Tavor, I. (2022). Act natural: Functional connectivity from naturalistic stimuli fMRI outperforms resting-state in predicting brain activity. *NeuroImage*, *258*(119359), 119359. https://doi.org/10.1016/j.neuroimage.2022.119359

Göttler, J., Kaczmarz, S., Kallmayer, M., Wustrow, I., Eckstein, H.-H., Zimmer, C., Sorg, C., Preibisch, C., & Hyder, F. (2019). Flow-metabolism uncoupling in patients with asymptomatic unilateral carotid artery stenosis assessed by multi-modal magnetic resonance imaging. *Journal of Cerebral Blood Flow and Metabolism: Official Journal of the International Society of Cerebral Blood Flow and Metabolism*, *39*(11), 2132–2143. https://doi.org/10.1177/0271678X18783369

Goyal, M. S., Blazey, T. M., Su, Y., Couture, L. E., Durbin, T. J., Bateman, R. J., Benzinger, T. L.-S., Morris, J. C., Raichle, M. E., & Vlassenko, A. G. (2019). Persistent metabolic youth in the aging female brain. *Proceedings of the National Academy of Sciences of the United States of America*, *116*(8), 3251–3255. https://doi.org/10.1073/pnas.1815917116

Gur, R. E., & Gur, R. C. (1990). Gender differences in regional cerebral blood flow. *Schizophrenia Bulletin*, *16*(2), 247–254. https://doi.org/10.1093/schbul/16.2.247

Gyurkovics, M., Clements, G. M., Low, K. A., Fabiani, M., & Gratton, G. (2021). The impact of 1/f activity and baseline correction on the results and interpretation of time-frequency analyses of EEG/MEG data: A cautionary tale. *NeuroImage*, *237*(118192), 118192. https://doi.org/10.1016/j.neuroimage.2021.118192

Imperatori, C., Panno, A., Giacchini, M., Massullo, C., Carbone, G. A., Clerici, M., Farina, B., & Dakanalis, A. (2020). Electroencephalographic correlates of body shape concerns: an eLORETA functional connectivity study. *Cognitive Neurodynamics*, *14*(5), 723–729. https://doi.org/10.1007/s11571-020-09618-1

Jausovec, N., & Jausovec, K. (2010). Resting brain activity: differences between genders. *Neuropsychologia*, *48*(13), 3918–3925. https://doi.org/10.1016/j.neuropsychologia.2010.09.020

Jenkinson, M., Beckmann, C. F., Behrens, T. E. J., Woolrich, M. W., & Smith, S. M. (2012). FSL. *NeuroImage*, *62*(2), 782–790. https://doi.org/10.1016/j.neuroimage.2011.09.015

Kaczmarz, S., Hyder, F., & Preibisch, C. (2020). Oxygen extraction fraction mapping with multi-parametric quantitative BOLD MRI: reduced transverse relaxation bias using 3D-GraSE imaging. *NeuroImage*, 117095. https://doi.org/10.1016/j.neuroimage.2020.117095

Kannurpatti, S. S., Motes, M. A., Rypma, B., & Biswal, B. B. (2011). Increasing measurement accuracy of age-related BOLD signal change: minimizing vascular contributions by resting-state-fluctuation-of-amplitude scaling. *Human Brain Mapping*, *32*(7), 1125–1140. https://doi.org/10.1002/hbm.21097

Kostanyan, A., & Nazaryan, K. (1992). Rat brain glycolysis regulation by estradiol-17 beta. *Biochimica et Biophysica Acta*, *1133*(3), 301–306. https://doi.org/10.1016/0167-4889(92)90051-c

Kudomi, N., Hirano, Y., Koshino, K., Hayashi, T., Watabe, H., Fukushima, K., Moriwaki, H., Teramoto, N.,

Iihara, K., & Iida, H. (2013). Rapid quantitative CBF and CMRO(2) measurements from a single PET scan with sequential administration of dual (15)O-labeled tracers. *Journal of Cerebral Blood Flow and Metabolism: Official Journal of the International Society of Cerebral Blood Flow and Metabolism*, *33*(3), 440–448. https://doi.org/10.1038/jcbfm.2012.188

Lachaux, J.-P., Fonlupt, P., Kahane, P., Minotti, L., Hoffmann, D., Bertrand, O., & Baciu, M. (2007). Relationship between task-related gamma oscillations and BOLD signal: new insights from combined fMRI and intracranial EEG. *Human Brain Mapping*, *28*(12), 1368–1375. https://doi.org/10.1002/hbm.20352

Lee, M. H., Smyser, C. D., & Shimony, J. S. (2013). Resting-state fMRI: a review of methods and clinical applications. *AJNR. American Journal of Neuroradiology*, *34*(10), 1866–1872. https://doi.org/10.3174/ajnr.A3263

Leenders, K. L., Perani, D., Lammertsma, A. A., Heather, J. D., Buckingham, P., Healy, M. J., Gibbs, J. M., Wise, R. J., Hatazawa, J., & Herold, S. (1990). Cerebral blood flow, blood volume and oxygen utilization. Normal values and effect of age. *Brain: A Journal of Neurology*, *113 (Pt 1)*, 27–47. https://doi.org/10.1093/brain/113.1.27

Liu, Z., de Zwart, J. A., Chang, C., Duan, Q., van Gelderen, P., & Duyn, J. H. (2014). Neuroelectrical decomposition of spontaneous brain activity measured with functional magnetic resonance imaging. *Cerebral Cortex (New York, N.Y.: 1991)*, *24*(11), 3080–3089. https://doi.org/10.1093/cercor/bht164

Lu, H., Xu, F., Rodrigue, K. M., Kennedy, K. M., Cheng, Y., Flicker, B., Hebrank, A. C., Uh, J., & Park, D. C. (2011). Alterations in cerebral metabolic rate and blood supply across the adult lifespan. *Cerebral Cortex (New York, N.Y.: 1991)*, *21*(6), 1426–1434. https://doi.org/10.1093/cercor/bhq224

Malmivuo, J., Suihko, V., & Eskola, H. (1997). Sensitivity distributions of EEG and MEG measurements. *IEEE Transactions on Bio-Medical Engineering*, *44*(3), 196–208. https://doi.org/10.1109/10.554766

Mannella, P., & Brinton, R. D. (2006). Estrogen receptor protein interaction with phosphatidylinositol 3-kinase leads to activation of phosphorylated Akt and extracellular signal-regulated kinase 1/2 in the same population of cortical neurons: a unified mechanism of estrogen action. *The Journal of Neuroscience: The Official Journal of the Society for Neuroscience*, *26*(37), 9439–9447. https://doi.org/10.1523/JNEUROSCI.1443-06.2006

Markello, R. D., Hansen, J. Y., Liu, Z.-Q., Bazinet, V., Shafiei, G., Suárez, L. E., Blostein, N., Seidlitz, J., Baillet, S., Satterthwaite, T. D., Chakravarty, M. M., Raznahan, A., & Misic, B. (2022). Neuromaps: Structural and functional interpretation of brain maps. *Nature Methods*, *19*(11), 1472–1479. https://doi.org/10.1038/s41592-022-01625-w

Ma, Y., Sun, H., Cho, J., Mazerolle, E. L., Wang, Y., & Pike, G. B. (2020). Cerebral OEF quantification: A comparison study between quantitative susceptibility mapping and dual-gas calibrated BOLD imaging. *Magnetic Resonance in Medicine*, *83*(1), 68–82. https://doi.org/10.1002/mrm.27907

Nagata, K., Tagawa, K., Hiroi, S., Shishido, F., & Uemura, K. (1989). Electroencephalographic correlates of blood flow and oxygen metabolism provided by positron emission tomography in patients with cerebral infarction. *Electroencephalography and Clinical Neurophysiology*, *72*(1), 16–30. https://doi.org/10.1016/0013-4694(89)90027-8

Nentwich, M., Ai, L., Madsen, J., Telesford, Q. K., Haufe, S., Milham, M. P., & Parra, L. C. (2020). Functional connectivity of EEG is subject-specific, associated with phenotype, and different from fMRI. *NeuroImage*, *218*(117001), 117001. https://doi.org/10.1016/j.neuroimage.2020.117001

Neuner, I., Arrubla, J., Werner, C. J., Hitz, K., Boers, F., Kawohl, W., & Shah, N. J. (2014). The default mode network and EEG regional spectral power: a simultaneous fMRI-EEG study. *PloS One*, *9*(2), e88214. https://doi.org/10.1371/journal.pone.0088214

Nezafati, M., Temmar, H., & Keilholz, S. D. (2020). Functional MRI Signal Complexity Analysis Using Sample Entropy. *Frontiers in Neuroscience*, *14*, 700. https://doi.org/10.3389/fnins.2020.00700

Nolte, G., Bai, O., Wheaton, L., Mari, Z., Vorbach, S., & Hallett, M. (2004). Identifying true brain interaction from EEG data using the imaginary part of coherency. *Clinical Neurophysiology: Official Journal of the International Federation of Clinical Neurophysiology*, *115*(10), 2292–2307. https://doi.org/10.1016/j.clinph.2004.04.029

Phadikar, S., Pusuluri, K., Iraji, A., & Calhoun, V. D. (2025). Integrating fMRI spatial network dynamics and EEG spectral power: insights into resting state connectivity. *Frontiers in Neuroscience*, *19*. https://doi.org/10.3389/fnins.2025.1484954

Raichle, M. E., MacLeod, A. M., Snyder, A. Z., Powers, W. J., Gusnard, D. A., & Shulman, G. L. (2001). A default mode of brain function. *Proceedings of the National Academy of Sciences of the United States of America*, *98*(2), 676–682. https://doi.org/10.1073/pnas.98.2.676

Rettberg, J. R., Yao, J., & Brinton, R. D. (2014). Estrogen: a master regulator of bioenergetic systems in the brain and body. *Frontiers in Neuroendocrinology*, *35*(1), 8–30. https://doi.org/10.1016/j.yfrne.2013.08.001

Scheeringa, R., Petersson, K. M., Kleinschmidt, A., Jensen, O., & Bastiaansen, M. C. M. (2012). EEG α power modulation of fMRI resting-state connectivity. *Brain Connectivity*, *2*(5), 254–264. https://doi.org/10.1089/brain.2012.0088

Shokri-Kojori, E., Tomasi, D., Alipanahi, B., Wiers, C. E., Wang, G.-J., & Volkow, N. D. (2019). Correspondence between cerebral glucose metabolism and BOLD reveals relative power and cost in human brain. *Nature Communications*, *10*(1), 690. https://doi.org/10.1038/s41467-019-08546-x

Sobel, M. E. (1982). Asymptotic confidence intervals for indirect effects in structural equation models. *Sociological Methodology*.

Sotero, R. C., & Trujillo-Barreto, N. J. (2008). Biophysical model for integrating neuronal activity, EEG, fMRI and metabolism. *NeuroImage*, *39*(1), 290–309. https://doi.org/10.1016/j.neuroimage.2007.08.001

St. Louis, E. K., Frey, L. C., Britton, J. W., Hopp, J. L., Korb, P., Koubeissi, M. Z., Lievens, W. E., & Pestana-Knight, E. M. (2016). *Introduction*. American Epilepsy Society. https://www.ncbi.nlm.nih.gov/books/NBK390346/

Tadel, F., Baillet, S., Mosher, J. C., Pantazis, D., & Leahy, R. M. (2011). Brainstorm: a user-friendly application for MEG/EEG analysis. *Computational Intelligence and Neuroscience*, *2011*, 879716. https://doi.org/10.1155/2011/879716

Theriault, J. E., Shaffer, C., Dienel, G. A., Sander, C. Y., Hooker, J. M., Dickerson, B. C., Barrett, L. F., & Quigley, K. S. (2023). A functional account of stimulation-based aerobic glycolysis and its role in interpreting BOLD signal intensity increases in neuroimaging experiments. *Neuroscience and Biobehavioral Reviews*, *153*(105373), 105373. https://doi.org/10.1016/j.neubiorev.2023.105373

Tomasi, D., & Volkow, N. D. (2010). Functional connectivity density mapping. *Proceedings of the National Academy of Sciences of the United States of America*, *107*(21), 9885–9890. https://doi.org/10.1073/pnas.1001414107

Tomasi, D., & Volkow, N. D. (2011). Functional connectivity hubs in the human brain. *NeuroImage*, *57*(3), 908–917. https://doi.org/10.1016/j.neuroimage.2011.05.024

Tomasi, D., Wang, G.-J., & Volkow, N. D. (2013). Energetic cost of brain functional connectivity. *Proceedings of the National Academy of Sciences of the United States of America*, *110*(33), 13642–13647. https://doi.org/10.1073/pnas.1303346110

Tsvetanov, K. A., Henson, R. N. A., & Rowe, J. B. (2021). Separating vascular and neuronal effects of age on fMRI BOLD signals. *Philosophical Transactions of the Royal Society of London. Series B, Biological Sciences*, *376*(1815), 20190631. https://doi.org/10.1098/rstb.2019.0631

Tu, W., Cramer, S. R., & Zhang, N. (2024). Disparity in temporal and spatial relationships between resting-state electrophysiological and fMRI signals. *eLife*, *13*. https://doi.org/10.7554/elife.95680.3

Vaishnavi, S. N., Vlassenko, A. G., Rundle, M. M., Snyder, A. Z., Mintun, M. A., & Raichle, M. E. (2010).

Regional aerobic glycolysis in the human brain. *Proceedings of the National Academy of Sciences of the United States of America*, *107*(41), 17757–17762. https://doi.org/10.1073/pnas.1010459107

Wang, Y., Wang, R., & Xu, X. (2017). Neural energy supply-consumption properties based on Hodgkin-Huxley model. *Neural Plasticity*, *2017*, 6207141. https://doi.org/10.1155/2017/6207141

Wang, Z. (2021). The neurocognitive correlates of brain entropy estimated by resting state fMRI. *NeuroImage*, *232*, 117893. https://doi.org/10.1016/j.neuroimage.2021.117893

White, R. E. (2002). Estrogen and vascular function. *Vascular Pharmacology*, *38*(2), 73–80. https://doi.org/10.1016/s0306-3623(02)00129-5

Whitfield-Gabrieli, S., & Nieto-Castanon, A. (2012). Conn: a functional connectivity toolbox for correlated and anticorrelated brain networks. *Brain Connectivity*, *2*(3), 125–141. https://doi.org/10.1089/brain.2012.0073

Wirsich, J., Amico, E., Giraud, A.-L., Goñi, J., & Sadaghiani, S. (2020). Multi-timescale hybrid components of the functional brain connectome: A bimodal EEG-fMRI decomposition. *Network Neuroscience (Cambridge, Mass.)*, *4*(3), 658–677. https://doi.org/10.1162/netn_a_00135

Wirsich, J., Jorge, J., Iannotti, G. R., Shamshiri, E. A., Grouiller, F., Abreu, R., Lazeyras, F., Giraud, A.-L., Gruetter, R., Sadaghiani, S., & Vulliémoz, S. (2021). The relationship between EEG and fMRI connectomes is reproducible across simultaneous EEG-fMRI studies from 1.5T to 7T. *NeuroImage*, *231*, 117864. https://doi.org/10.1016/j.neuroimage.2021.117864

Zhang, J., Cho, J., Zhou, D., Nguyen, T. D., Spincemaille, P., Gupta, A., & Wang, Y. (2018). Quantitative susceptibility mapping-based cerebral metabolic rate of oxygen mapping with minimum local variance. *Magnetic Resonance in Medicine*, *79*(1), 172–179. https://doi.org/10.1002/mrm.26657

Zhong, X. Z., & Chen, J. J. (2022). Resting-state functional magnetic resonance imaging signal variations in aging: The role of neural activity. *Human Brain Mapping*, *43*(9), 2880–2897. https://doi.org/10.1002/hbm.25823

Zhong, X. Z., Polimeni, J. R., & Chen, J. J. (2024). Predicting the macrovascular contribution to resting-state fMRI functional connectivity at 3 Tesla: A model-informed approach. *Imaging Neuroscience*, *2*, 1–22. https://doi.org/10.1162/imag_a_00315

Zhong, X. Z., Tong, Y., & Chen, J. J. (2024). Assessment of the macrovascular contribution to resting-state fMRI functional connectivity at 3 Tesla. *Imaging Neuroscience*, *2*, 1–20. https://doi.org/10.1162/imag_a_00174

Zhong, X. Z., Van Lankveld, H., & Chen, J. J. (2025). The link to oxidative metabolism varies across rs-fMRI metrics: A whole-brain assessment using macrovascular correction. In *bioRxiv*. https://doi.org/10.1101/2025.02.11.633958

Zhong, X. Z., Van Lankveld, H., Mathew, A., & Chen, J. J. (2025). The link between steady-state EEG and rs-fMRI metrics in healthy young adults: the effect of macrovascular correction. In *bioRxiv* (p. 2025.06. 06.658306). https://doi.org/10.1101/2025.06.06.658306

Zhu, J., Zhou, Y., Jin, B., & Shu, J. (2023). Role of estrogen in the regulation of central and peripheral energy homeostasis: from a menopausal perspective. *Therapeutic Advances in Endocrinology and Metabolism*, *14*, 20420188231199359. https://doi.org/10.1177/20420188231199359

Znamensky, V., Akama, K. T., McEwen, B. S., & Milner, T. A. (2003). Estrogen levels regulate the subcellular distribution of phosphorylated Akt in hippocampal CA1 dendrites. *The Journal of Neuroscience: The Official Journal of the Society for Neuroscience*, *23*(6), 2340–2347. https://doi.org/10.1523/jneurosci.23-06-02340.2003